Journal of Electronic Materials (2024) 53:5018–5027
https://doi.org/10.1007/s11664-024-11054-4

28TH INTERNATIONAL CONFERENCE ON NUCLEAR TRACKS AND RADIATION MEASUREMENTS

Analysis of Various Properties of PMMA/PS Polymer Blends

Harsh D. Patel[1] · **Naveen K. Acharya**[1]

Received: 7 December 2023 / Accepted: 18 March 2024 / Published online: 22 April 2024

Abstract

Differential scanning calorimetry (DSC) is considered one of the most versatile thermal analysis tools for characterizing polymer samples. This paper reports a DSC study of blends of polymethyl methacrylate (PMMA) and polystyrene (PS) prepared in different ratios by weight percentage for all blend ratios used for PMMA:PS (80:20, 60:40, 50:50, 60:40, 20:80) using the solution cast method. The samples were analyzed at heating rates of 5°C/min, 10°C/min and 20°C/min in the temperature range of 50–200°C. The glass transition temperature (T_g) was theoretically calculated using Fox's equation for all the samples. It was found that the experimental glass transition temperature is very close to the theoretical values. DSC thermograms supported the confirmation of the formation of PS–PMMA blends and demonstrated a significant change in their thermal behavior with changes in blend ratio. The activation energy of crystallization was evaluated using both isokinetic and iso-conversional approaches, and similar findings were found. Using various iso-conversional approach models, the activation was determined for pure and blended polymers through their glass transition. Notably, the activation energy values obtained using different iso-conversional methods and specific iso-conversional techniques, such as Ozawa, Kissinger, Boswell, and Augis and Bennett, are relatively consistent.

Graphical Abstract

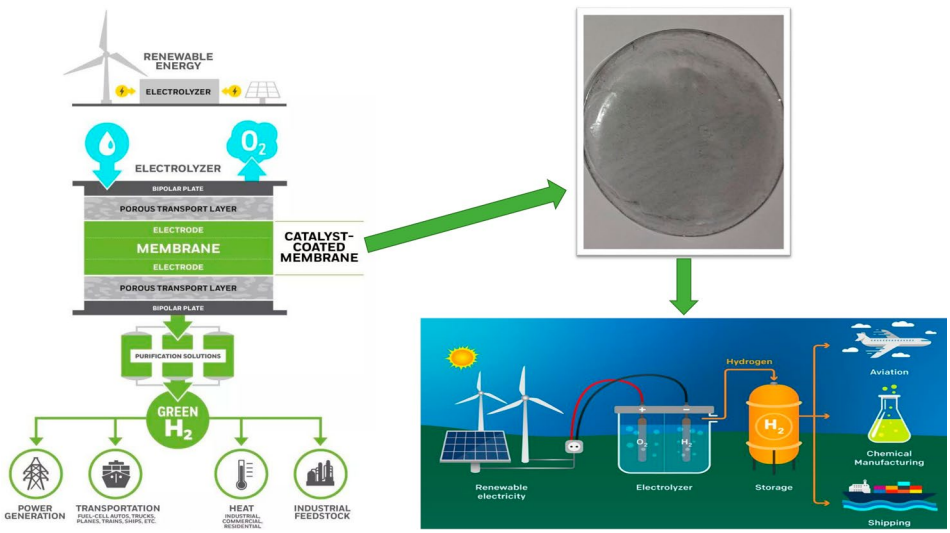

Keywords Thermal analysis · polymer blends · differential scanning calorimetry · glass transition

✉ Harsh D. Patel
harshpatel10996@gmail.com

Naveen K. Acharya
sarnavee@gmail.com

[1] Applied Physics Department, Faculty of Technology and Engineering, The M.S. University of Baroda, Vadodara 390001, India

Introduction

A polymeric material's processing temperature and end-use properties are determined by its glass transition temperature, T_g, which identifies the temperature at which the material undergoes a change in phase behavior. At or below T_g, the polymeric structure is hard, brittle, and glassy,[1,2] whereas it remains soft and viscous above this point. One of the most suitable thermal analysis techniques for identifying a material's glass transition temperature is differential scanning calorimetry (DSC). Using a thermal analysis of DSC, researchers have identified polymer melting points (T_m) and glass transition points (T_g).[3–6] Many polymers have standard melting points and glass transition temperatures. DSC tests indicate likely polymer breakdown by a decline in the predicted melting point (T_m), which depends on the polymer's molecular weight. As a result, lesser-grade polymers are likely to have lower melting points than reference polymers of higher molecular weight. DSC is also helpful in determining the concentrations of specific polymers and medicines.[7] The Gibbs free energy of mixing, which may be measured in terms of interaction energy, combinatorial entropy, and compressibility, must be negative. Its second derivative must be positive for a miscible polymer blend to be stable. The DSC is a sophisticated device that was created to measure energy directly and permits exact heat capacity measurements. When a polymer changes from a glassy to a rubbery state, it changes its hardness, volume, and percent elongation to break.[8] The glass transition temperature is influenced by several variables: (1) Increased surrounding pressure due to a reduction in free volume may also cause a high T_g. (2) When plasticizer is mixed into a polymer, the free volume in the material structure increases, causing polymer chains to move about at lower temperatures, decreasing the T_g of the polymer. (3) The polar group, molecular structure, molecular weight and chemical cross-linking are all part of the polymer's chemical structure. (4) This also explains why amorphous materials have greater entropy values, and crystalline materials have lower entropy values.[9–12] The greater the entropy, the higher the glass transition temperature (T_g).[12–16]

The thermal analysis of polystyrene (PS), polymethyl methacrylate (PMMA), and PMMA/PS mix samples has been conducted using the DSC method. The T_g has been calculated and the changes seen in mixing PMMA and PS have been interpreted. When PMMA and PS are blended, the T_g of PS changes and the appearance of a single peak demonstrates that the two polymers are miscible. The synthesis of PMMA/PS blend was further confirmed by DSC plots, which revealed a considerable shift in thermal behavior. The DSC analysis of PMMA, PS and blend of PMMA/PS films made with various weight percentage (wt.%) ratios is presented in this work. The DSC test depicts the miscibility behavior of polymer blends and composites by monitoring the glass transition temperature for all blend ratios utilized for PMMA:PS (80:20, 60:40, 50:50, 60:40, and 20:80). Analysis by Akahira et al.[17] shows that the morphological structure of PMMA, PS and PMMA/PS blends are impacted by the glass transition behavior of the polymer systems. In PMMA and PS blends, the T_g of PS increases as the percentage of PS in these blends decreases. When the amorphous component in the composition changes, results show that T_g mainly depends on the physical state of the semi-crystalline domains in the composition. Combining polymers alters their thermal diffusivity, capacity, density, thermal conductivity and specific heat in dramatic ways.[18–20]

Theory

Many approaches have been devised to analyze the crystallization process; most of them use Kolmogorov, Johnson, Mehl, and Avrami's (KJMA) transformation rate equation.[10] This equation is obtained through isothermal tests and is written as Eq. 1:

$$\frac{d\alpha}{dt} = nK(1-\alpha)[-\ln(1-\alpha)]^{(1-n)/n}, \tag{1}$$

where α is the Avrami exponent (also known as growth exponent), and K is the rate constant in the form of Arrhenius temperature at a particular time $K(T)$. The rate constant is calculated as follows:

$$K(T) = k_0 \exp\left(\frac{-E}{RT}\right), \tag{2}$$

where the pre-exponential factor is k_0, the activation energy is E, and the universal gas constant is R.

For reactions associated with linear growth exposed to various circumstances, the KJMA rate in Eq. 2, based on several key assumptions, seems to be valid.[21]

Experimental Set-Up

Synthesis of Membrane

Polymer and pre-polymer were dissolved in a suitable solution. The pure polymeric films of PMMA and PS and the blend membrane films of PMMA/PS were prepared by the solution casting method, which is shown in Fig. 1.[5–7,22,23] A glass plate magnetic stirrer was used for solution casting of dichloromethane onto the majority of the blend films.

To obtain a homogeneous solution, the solutions of PMMA and PS were individually stirred for 3 h, and then the mixture of PMMA/PS was again stirred for 24 h at

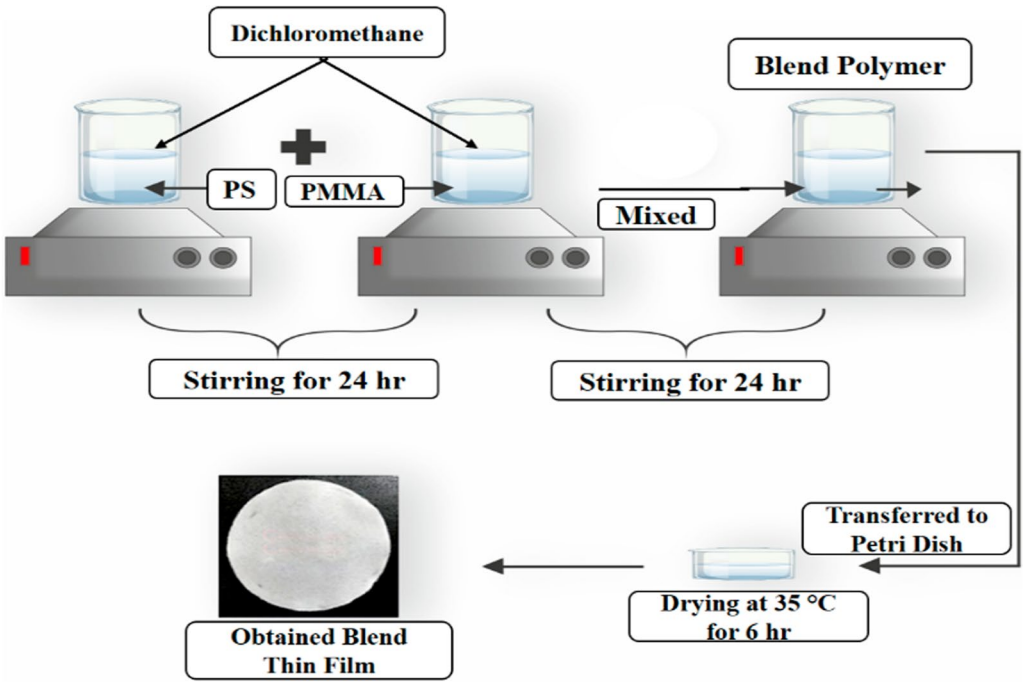

Fig. 1 Synthesis of polymer blend membranes by solution casting method.

ambient temperature. On a flat-bottomed glass, the mixture was transferred, and the solvent was allowed to evaporate overnight in the system.

Characterization of Membrane

The thermal analysis and glass transition temperatures of pure and blended polymers were obtained by using a DSC-25 (TA Instruments, USA) system. Here, we scanned film at heating rates of 5°C/min, 10°C/min and 20°C/min, with accuracy of ±1 °C. The sample was heated to 160°C at 5°C/min for a scan that was used to clear the last scan's thermal history, and the same experiment was performed with 10°C/min and 20°C/min heating rates. Heat flow from 50°C to 160°C at different rates of 5°C/min, 10°C/min and 20°C/min was used to analyze specified samples. TRIOS software was used to find the glass transition temperatures and heat capacity. The glass transition temperatures and heat capacity measured by DSC 8500 were used to identify T_g, the point at which the heat capacity begins to change. Small bits of polymer thin film were cut and placed in aluminum pans. A micro weight balance was used to weigh the samples.[24–26] The DSC experiments were conducted using polymer film samples weighing between 2.5 mg and 3.8 mg. Samples consisted of PS, PMMA, and blends of PS/PMMA polymer in weight percent ratios of 80:20, 60:40, 50:50, 40:60, and 20:80. The sample testing process was carried out three or four times, each time with a different heating rate and sample from the batch.

Results and Discussions

PMMA and PS blends were developed by modifying the molecular weights of PMMA to prevent solvent-induced crystals from forming. Two T_g overlapped in PS/PMMA immiscible blends of 93°C and 100°C. The DSC thermograms showed that the PS melting peak was not visible in these blends. At all compositions, the blend films were transparent for PS/PMMA.[25–27] Blends were heated at a temperature up to 90°C above T_g for a week before cooling to room temperature and then quenching to see whether they were miscible at equilibrium. The films were still transparent and showed the same T_g as previously. According to these observations, all of the PS/PMMA (80:20), PS/PMMA (50:50), and PS/PMMA (40:60) blends are miscible while in equilibrium. These results are shown in Fig. 2a–g.

Figure 2a–g show the weight percentage (wt.%) values for pure polymers and the different weight ratios for PS/PMMA polymer blends. A DSC experiment was conducted to examine the impact of PMMA in the PMMA/PS blends with various concentrations on the T_g value.[28,29] Here, Fig. 2a and b show the T_g value of pure PS and PMMA polymer with different heating rates. From this graph, it is observed that when we increase the heating rate temperature from 5°C/m to 20°C/min, the glass transition temperature is also increased according to that heating rate. From the T_g values of PS/PMMA polymer blends shown in Fig. 2, it can be seen that the T_g changed as we changed different wt.% ratios of miscible polymer blends. This happens because

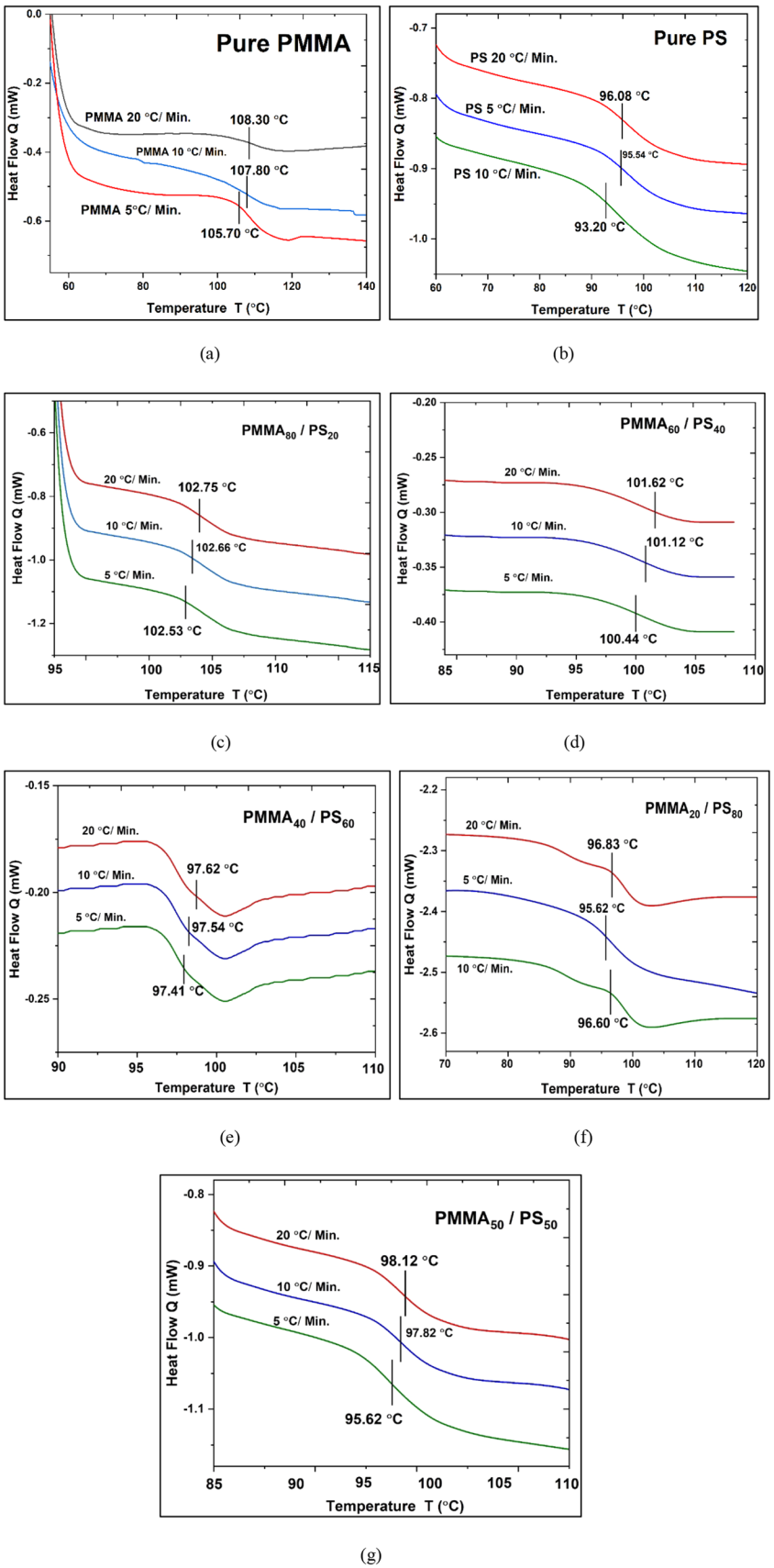

Fig. 2 (a–g) DSC thermograms of pure PMMA, pure PS and blends of PS/PMMA with different heating rates.

of miscible bonding between PS and PMMA polymer.[29] Figure 2a–g indicate that the T_g values of these blends lay between the T_g values of the pure polymer and were well estimated by Fox's equation. Also, for a given range of molecular weights, the Flory–Fox equation may be used to simulate how the glass transition temperature varies with the choice of plasticizers, or how low-molecular-weight diluents may be added to alter a polymer's glass transition temperature.[27–30] Lower T_g is possible because the addition of molecular weight, which raises the system's free volume, reduces its melting point. The Fox equation (Eq. 3) helps explain this phenomenon:

$$\frac{1}{T_g} = \frac{W_1}{T_{g1}} + \frac{W_2}{T_{g2}}, \tag{3}$$

where w_1 and $w_2$are the weight fractions and T_{g1} and T_{g2} are the glass transition temperatures of polymer-1 and polymer-2, respectively. When it comes to predicting glass transition temperatures in (miscible) polymer blends and statistical copolymers, the accuracy of the Fox Eq. 3 is generally fairly high.[27] The values of T_g are obtained from the DSC instrument and T_g calculated through Fox's Eq. 3.

From Table I it is observed that the values of T_g obtained from DSC thermograms using TRIOS software are almost the same as the values of T_g calculated by using Fox's Eq. 3. To blend thin film with a ratio of $PMMA_{50}$–PS_{50}, the experimental value of T_g is around 97.82°C, and 98.12°C is obtained through the Fox equation. Hence, these results are a verification of Fox's equation, which also confirms the observed behavior of heterogeneous polymeric systems.[31]

Iso-Conversional Methods

The iso-conversional methods are independent of the reaction model and give reliable activation energy values. They are classified as differential and integral methods. The iso-conversional techniques are based on the basic kinetic equation (Eq. 4).[31–33]

$$\frac{d\alpha}{dt} = K(T)f(\alpha), \tag{4}$$

where $K(T)$ is the rate constant given by Eq. 2 and is the reaction model in terms of KJMA formalism Eq. 1. The integral form of Eq. 4 can be expressed as:

$$g(\alpha) = \int_0^{\alpha} [f(\alpha)]^{-1} d\alpha = \frac{k_0}{\beta} \int_0^{T} \exp\left(\frac{-E}{RT}\right) dT. \tag{5}$$

Due to the unavailability of the exact solution of the temperature integral in Eq. 5, several approximations have been made, which resulted in different methods.[30–32]

Approaches to Iso-Conversion Based on Linear Integrals

Ozawa–Flynn–Wall (OFW) Method

To simplify the temperature integral in Eq. 5, Ozawa, Flynn, and Wall employed an estimate proposed by Doyle in their technique[33] :

$$\ln \beta = -1.0516 \frac{E_\alpha}{RT_\alpha} + \text{const.} \tag{6}$$

The slope of ln (β) versus $1/T_\alpha$ yields −1.0516, which may be used to compute the activation energy. The same may be said for $T = T_p$ (Ozawa method).

The amount of energy taken by a collection of atoms in the glassy region to move from one state to another is known as the glass transition activation energy. Here, we can find the activation energy by using this Ozawa–Flynn–Wall (OFW) plot, shown in Fig. 3. The activation energy of pure PS is 86.41 E/kJ mol^{-1} and for pure PMMA it is 212.30 E/kJ mol^{-1}.[34] When we increased the wt.% of PMMA in the PMMA/PS blend, the activation energy increased to a greater degree than in PS, but not above the activation energy of PMMA. This happened because of the miscible and glassy behavior of both polymers.

Table I Comparison of T_g values through DSC experiments and calculated using Fox's equation (Eq. 3)

Variation in temp. ramp rate	Pure PMMA	Pure PS	$PMMA_{80}$–PS_{20}		$PMMA_{60}$–PS_{40}		$PMMA_{50}$–PS_{50}		$PMMA_{40}$–PS_{60}		$PMMA_{20}$–PS_{80}	
	Exp.	Exp.	Exp.	Calc.	Exp.	Calc.	Exp.	Calc.	Exp.	Calc.	Exp.	Calc.
T_g (°C), ramp rate 5 °C/min	108.90	96.08	102.75	104.72	101.62	102.34	98.12	98.18	94.62	97.06	96.83	96.87
T_g (°C), ramp rate 10 °C/min	107.80	95.54	102.66		101.12		97.82		97.64		95.62	
T_g (°C), ramp rate 15 °C/min	105.70	93.20	102.53		100.44		95.62		97.41		96.60	

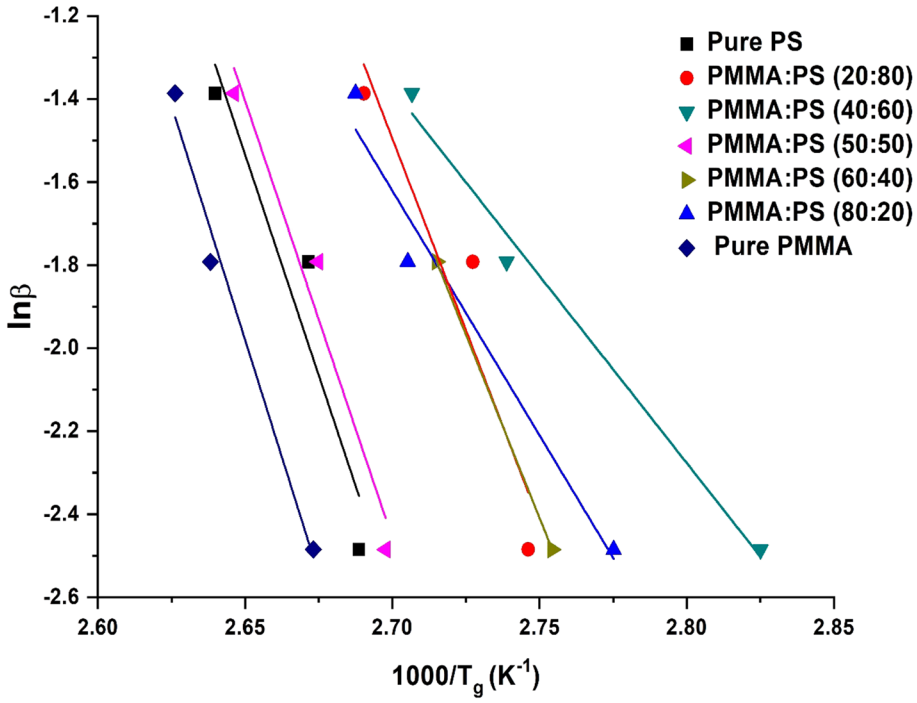

Fig. 3 Ozawa–Flynn–Wall (OFW) plot of pure and blends of PMMA/PS polymer membranes.

Kissinger–Akahira–Sunose (KAS) Method

Because the precise solution of the temperature integral in Eq. 4 is not available, Coats and Redfern[35] provided an estimate in their paper employed in this KAS technique. This technique assumes that the rate of reaction is most significant at the peak temperature (T_p), implying a constant degree of conversion (α) at T_p. The Kissinger formula is as follows:

$$\ln\left(\frac{\beta}{T_P^2}\right) = -\frac{E}{RT_P} + \ln\left(\frac{k_0 R}{E}\right). \tag{7}$$

Here, the activation energy from Fig. 4 is calculated on the plot of Kissinger–Akahira–Sunose (KAS). For pure PMMA it is 216.74 E/kJ mol^{-1} and for pure PS it is 88.68 E/kJ mol^{-1}. The activation energy increased as we increased the wt.% of PMMA in the blends of PMMA/PS. Moreover, from this plot, we can also observe as we go from pure PS to PMMA that the value of the intercept slope also increases: for PS its value is 10.21 and for PMMA it is 26.07. This graph shows that OFW and KAS results are near to one another, but Friedman's points are much more dispersed.[36]

Boswell Method

The activation energy at peak temperature (T_p) may be calculated using this approach proposed by Boswell:[36]

$$\ln\left(\frac{\beta}{T_P}\right) = -\frac{E}{RT_P} + \text{const}, \tag{8}$$

where E is the activation energy.

From this plot of Fig. 5 Boswell for membranes, we calculated activation energy for PS and PMMA and blends of PMMA/PS.[36] The value of activation energy (AE) for PS is 87.97 E/kJ mol^{-1} and the slope value is 10.56; for PMMA the AE value is 219.82 E/kJ mol^{-1} and the slope value is 26.02.

Augis and Bennett's Method

Augis and Bennett[37] indicated that this approach might be used for heterogeneous processes given by the Avrami expression (Eq. 7) as an extension of the Kissinger method. The onset temperature of characterization (T_0) is combined with the peak characterization temperature in this approach, yielding correct E values from Eq. 9:

$$\ln\left(\frac{\beta}{T_P - T_0}\right) = -\frac{E}{RT_P} + \ln k_0 \tag{9}$$

Here, the activation energy is calculated from Augis and Bennett's plot from Fig. 6. For pure PMMA, the AE is 221.81 E/kJ mol^{-1}, and for pure PS it is 92.27 E/kJ mol^{-1}. The value of activation energy increased as we increased the wt.% of PMMA in the blends of PMMA/PS.[37] Moreover, from this plot, we can also observe as we go from pure PS to

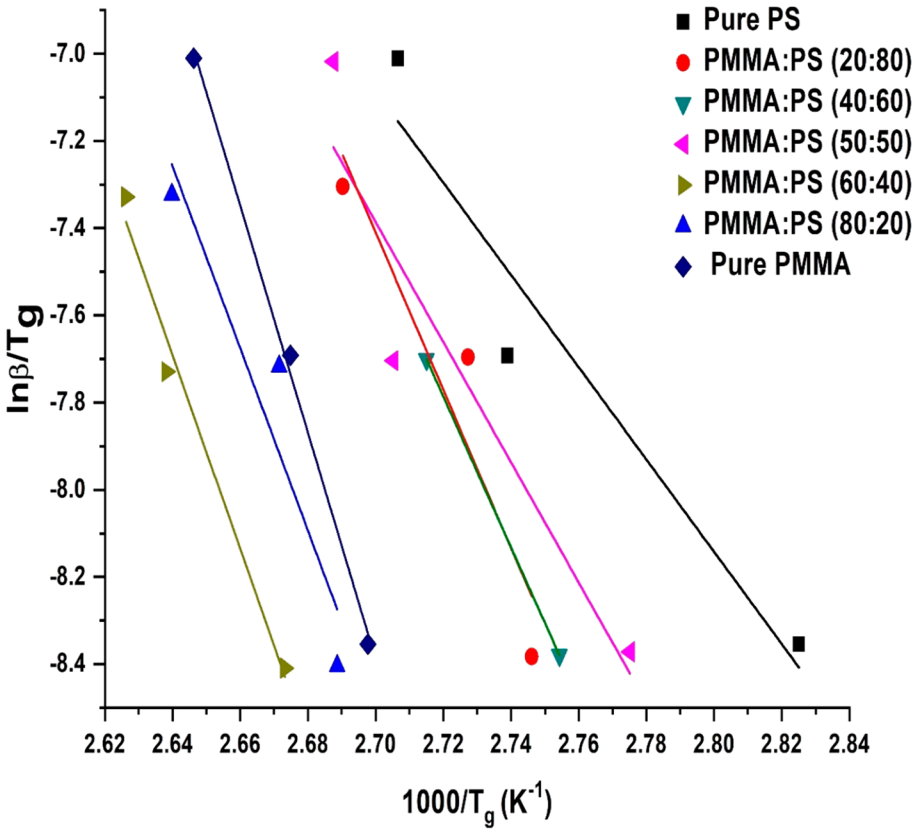

Fig. 4 Kissinger–Akahira–Sunose (KAS) plot of pure and blended PMMA/PS polymer membranes.

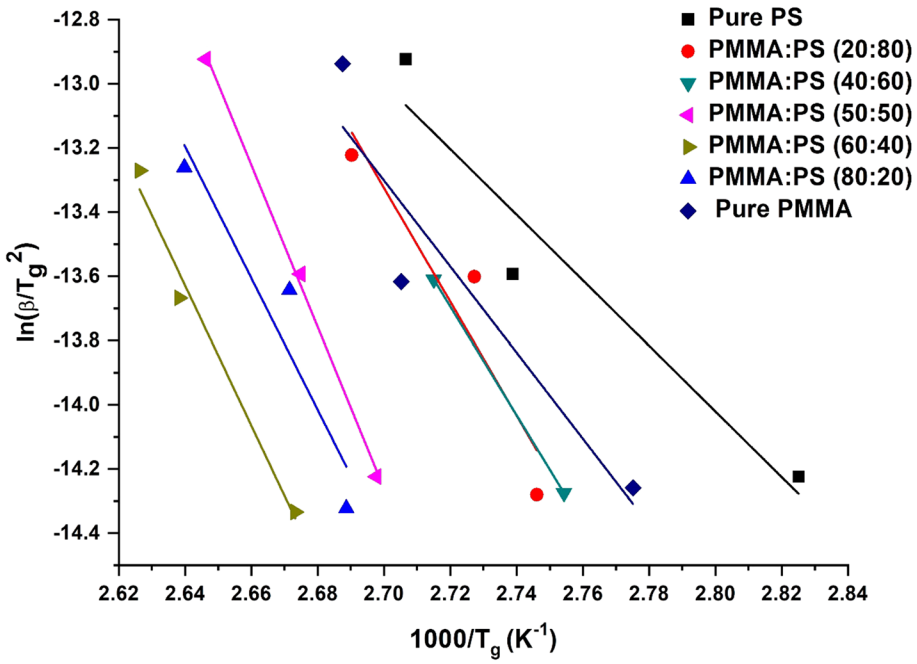

Fig. 5 Boswell plot of pure and blended PMMA/PS polymer membranes.

PMMA that the value of the intercept slope also increases; for PS its value is 10.89 and for PMMA it is 26.68.

Table II presents the activation energy of pure PS and PMMA and the blends of PMMA/PS calculated from iso-conversional method plots. The non-isothermal characterization kinetics of the present glassy polymer may thus be studied using Augis and Bennett's method. Using both iso-kinetic and iso-conversional approaches, the kinetics of

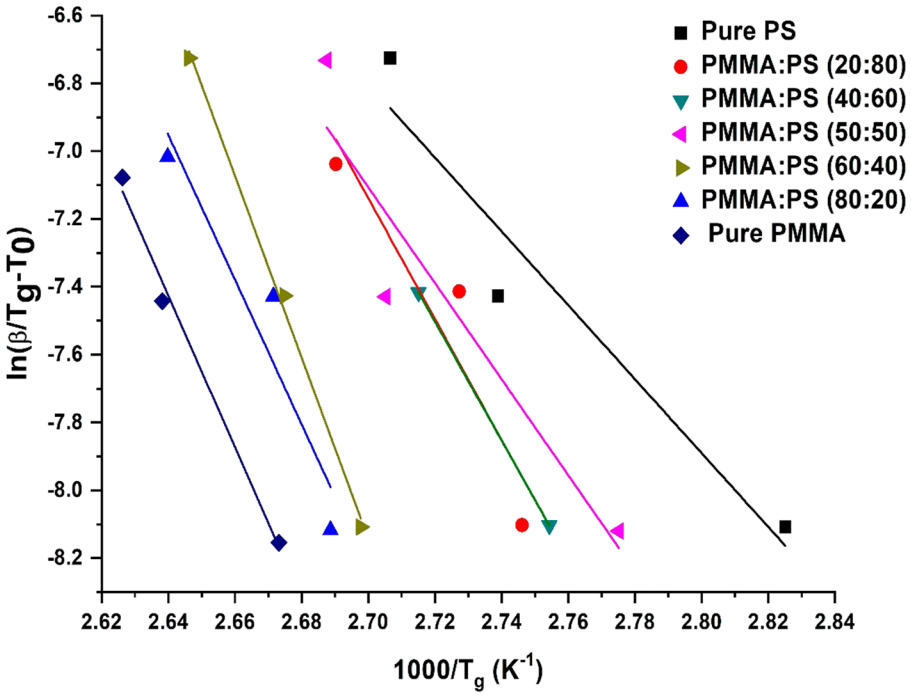

Fig. 6 Augis and Bennett's plot of pure and blended PMMA/PS polymer membranes.

Table II Activation energy of pure PS and PMMA and the blends of PMMA/PS calculated from iso-conversional method plots

Method	Pure PS	Pure PMMA	$PMMA_{80}$–PS_{20}	$PMMA_{60}$–PS_{40}	$PMMA_{50}$–PS_{50}	$PMMA_{60}$–PS_{40}	$PMMA_{20}$–PS_{80}
	E/kJ mol^{-1}						
Ozawa	86.41	212.03	178.51	168.0	146.10	139.53	111.79
Kissinger	84.88	216.74	181.49	170.43	147.49	140.67	111.49
Boswell	87.87	219.82	184.57	173.51	150.56	143.66	114.56
Augis and Bennett	90.27	221.81	185.81	177.25	148.4	145.57	117.64

characterization are examined. The activation energy and pre-exponential factor may be obtained using iso-conversional techniques (k_0). Because it does not use any mathematical approximation to simplify the temperature integral in Eq. 4, this approach for linear differential iso-conversion is believed to yield accurate estimates of the activation energy.[37] As a result, no assumptions about the reaction model are required. This indicates that the approach is unaffected by the reaction model.[38,39]

Conclusion

Blends of PMMA and PS are miscible in nature, as observed in DSC thermograms. Fox's formula for binary blends was found to be in excellent accord with this, confirming the state behavior of heterogeneous polymeric systems. PMMA, PS and PMMA/PS blends show the greatest temperature-dependent thermal conductivity and thermal diffusivity in the area of their respective polymer phase's glass transition point. PMMA phase T_g increases as a function of PS phase blends, whereas PS phase T_g changes drastically statistically. This is shown in the glass transition analysis of the analyzed polymeric blends of PMMA and PS. PMMA and PS blends were found to be extremely miscible.[40,41]

The activation energy of various blends was estimated using different theoretical models. The characterization kinetics of the initial peak of the characterization process in the experimental system was studied using all four model-dependent isokinetic and model-free iso-conversional approaches. Crystallization is a phase transition from an amorphous to a crystallized state, but it is possible that this principle may be used for glass-to-amorphous transformations as well. Notably, the activation energy values obtained using different iso-conversional methods and specific iso-conversional techniques, such as Ozawa, Kissinger, Boswell, and Augis and Bennett, are relatively consistent, and can be used to determine the relationship between activation energy and transformed fraction for pure PS and PMMA polymers and blends of PMMA/PS membranes.[41]

Acknowledgments The authors are thankful to the Applied Physics Department for providing the facility under the DST-FIST (SR/FST/PS-II/2017/20) scheme and DST-PURSE (SR/PURSE/PS- II/2018/28). Harsh Patel is also thankful to University Grants Commission, New Delhi, for providing Senior Research Fellowship (SRF) under NET-JRF Scheme (1217/(CSIR-UGC NET DEC. 2018)). Authors are also thankful to Research and Consultancy Cell, M.S University of Baroda for providing financial assistance (RDC/Dir./2023-24/19/28).

Author Contributions Conceptualization: [Harsh Patel, Naveen Acharya], Sample preparation [Harsh Patel] Methodology: [Harsh Patel, Naveen Acharya], Formal analysis and investigation: [Harsh Patel, Naveen Acharya], Writing—original draft preparation: [Harsh Patel, Naveen Acharya,], Supervision: [Naveen Acharya]

Data Availability The data that support the finding of this study are available from the corresponding author upon reasonable request

Conflict of interest The authors declare that they have no known competing financial interests or personal relationships that could have appeared to influence the work reported in this paper.

References

1. P. Amchova, H. Kotolova, and J. Ruda-Kucerova, Health safety issues of synthetic food colorants. *Regul. Toxicol. Pharm.* 73, 914 (2015).
2. A.G. Newsome, C.A. Culver, and R.B. Van Breemen, Nature's palette: the search for natural blue colorants. *J. Agr. Food Chem.* 62, 6498 (2014).
3. J. Burrows, Microbial pigments in the food industry—challenges and the way forward. *Compr. Rev. Food Sci. F.* 8, 394 (2009).
4. D. Miorandi, S. Sicari, F.D. Pellegrini, and I. Chlamtac, Internet of things: vision, applications, and research challenges. *Ad Hoc Netw.* 10, 1497–1516 (2012).
5. A.B. Giasuddin, S.R. Kanel, and H. Choi, Adsorption of humic acid onto nanoscale zerovalent iron and its effect on arsenic removal. *Environ. Sci. Technol.* 41, 2022 (2007).
6. X.R. Xu, H.-B. Li, W.-H. Wang, and J.-D. Gu, Decolorization of dyes and textile wastewater by potassium permanganate. *Chemosphere* 59, 893 (2005).
7. A.M. Kansara, S.G. Chaudhri, and P.S. Singh, A facile one-step preparation method of recyclable superhydrophobic polypropylene membrane for oil–water separation. *RSC Adv.* 6, 61129–61136 (2016).
8. R. Hassan, A.R. Dahy, S. Ibrahim, I. Zaafarany, and A. Fawzy, Oxidation of some macromolecules. Kinetics and mechanism of oxidation of methyl cellulose polysaccharide by permanganate ion in acid perchlorate solutions. *Ind. Eng. Chem. Res.* 51, 5424 (2012).
9. R. Hassan, S. Ibrahim, and S. Sayed, Kinetics and mechanistic aspects on electron-transfer process for permanganate oxidation of poly(ethylene glycol) in aqueous acidic solutions in the presence and absence of Ru(III) catalyst. *Int. J. Chem. Kinet.* 50, 775 (2018).
10. J. Whitson and P. Rabinovitch, Late-life restoration of mitochondrial function reverses cardiac dysfunction in old mice. *Elife* 9, 55513 (2020).
11. S.M. Ibrahim and A.F. Al-Hossainy, Oxidation process and kinetics of bromothymol blue by alkaline permanganate. *Int. J. Chem. Kinet.* 318, 114041 (2020).
12. A.M. Shaker, R.M. El-Khatib, and L.A. Nassr, Combined experimental and TDDFT-DFT computation, characterization, and optical properties for synthesis of keto-bromothymol blue dye thin film as optoelectronic devices. *Carbohyd. Polym.* 78, 710 (2009).
13. W. Zhang, X. Zhang, Z. Wu, K. Abdurahman, and D. Jia, Gas-sensing properties and preparation of waste mask fibers/ZnS composites. *Compos. Sci. Technol.* 188, 107966 (2019).
14. C. Di Valentin, G. Pacchioni, A. Selloni, S. Livraghi, and E. Giamello, Characterization of paramagnetic species in N-Doped TiO_2 powders by EPR spectroscopy and DFT calculations. *J. Phys. Chem. B* 109, 11414 (2005).
15. W. Chen, S. Cai, Q. Ren, W. Wen, and Y. Zhao, Recent advances in electrochemical sensing for hydrogen peroxide: a review. *Analyst* 137, 49–58 (2011).
16. A. Hussain, M.U. Khan, M. Ibrahim, M. Khalid, A. Ali, S. Hussain, M. Saleem, N. Ahmad, S. Muhammad, and A.G. Al-Sehemi, Exploration of noncovalent interactions, chemical reactivity, and nonlinear optical properties of piperidone derivatives: a concise theoretical approach. *J. Mol. Struct.* 1201, 127183 (2020).
17. R. Li, X. Tian, M. Wei, A.A. Dong, X. Pan, Y. He, and X. Song, s-Sensing properties and preparation of waste mask fibers/ZnS composites. *Compos. Commun.* 27, 100889 (2021).
18. Y. Zhao and D.G. Truhlar, Density functionals with broad applicability in chemistry. *Acc. Chem. Res.* 41, 157 (2008).
19. J.M. Rosa, E.B.A. Tambourgi, and J.C. Santana, Dyeing of cotton with reactive dyestufs: the continuous reuse of textile wastewater fuent treated by ultraviolet/hydrogen peroxide homogeneous photocatalysis. *J. Clean. Prod.* 90, 60–65 (2015).
20. C. Fang, D. Cen, Y. Wang, Y. Wu, and G. Han, ZnS@ ZIF-8 core-shell nanoparticles incorporated with ICG and TPZ to enable H2S-amplified synergistic therapy. *Theranostics* 10, 7671–7682 (2020).
21. W. Zhang, Z. Wu, J. Hu, Y. Cao, J. Guo, M. Long, H. Duan, and D. Jia, Flexible chemiresistive sensor of polyaniline coated filter paper prepared by spraying for fast and non-contact detection of nitroaromatic explosives. *Sens. Actuators B* 304, 127233.1-127233.9 (2020).
22. S. Kim, X. Yang, K. Yang, H. Guo, M. Cho, Y.J. Kim, and Y. Lee, Recycling respirator masks to a high-value product: from COVID-19 prevention to highly efficient battery separator. *Chem. Eng. J.* 430, 132723 (2022).
23. S. Rehman, S. Rafiq, N. Muhammad et al., Surface tuning of silica by deep eutectic solvent to synthesize biomass derived based membranes for gas separation to enhance the circular bioeconomy. *Fuel* 31, 122355–122378 (2022).
24. A.F. Al-Hossainy and A. Ibrahim, Reactivity trends of hydroxide ion attack on high spin Fe(II) complexes including bromosalicylidene amino acid ligands in some mixed aqueous solvents: Gibb's free energy of transfer and initial-transition state analysis. *Mat. Sci. Semicon. Proc.* 38, 13 (2015).
25. M.S. Manhas and F. Mohammed, A kinetic study of oxidation of β-cyclodextrin by permanganate in aqueous media. *Colloids Surf.* 295, 165 (2007).
26. S.H. Mohamed, Y.M. Issa, S.A. Elfeky, A.A. Ahmed, and N.S. Abdelkader, The synthesis, spectroscopic characterization, DFT/TD-DFT/PCM calculations of the molecular structure and NBO of the novel charge-transfer complexes of pyrazine Schiff base derivatives with aromatic nitro compounds. *J. Mol. Struct.* 1212, 128074 (2020).
27. L. Jiao, J.Y.R. Seow, W.S. Skinner, Z.U. Wang, and H.-L. Jiang, Metal–organic frameworks: structures and functional applications. *Mater. Today* 27, 43 (2019).
28. A. Al-Hossainy, M.S. Zoromba, O. El-Gammal, and F.I. El-Dossoki, Influence of gamma-irradiation on structural, optical and photocatalytic performance of TiO_2 nanoparticles under controlled atmospheres. *Struct. Chem.* 30, 1365 (2019).
29. M.F. Kaya, Ö. Bağlayan, E.G. Kaya, and Ö. Alver, Synthesis, spectroscopic characterization, and crystal structures of Schiff

bases derived from nicotinic hydrazide. *J. Mol. Struct.* 1149, 257 (2017).
30. D. Zhang, C. Jiang, P. Li, and Y. Sun, Layer-by-layer self-assembly of Co_3O_4 nanorod-decorated MoS_2 nanosheet-based nanocomposite toward high-performance ammonia detection. *ACS Appl. Mater. Interfaces* 9, 6462–6471 (2017).
31. A. Al-Hossainy, M.S. Zoromba, M. Abdel-Aziz, M. Bassyouni, A. Attar, M. Zwawi, A. Abd-Elmageed, H. Maddah, and A.B. Slimane, Fabrication of heterojunction diode using doped-poly (ortho-aminophenol) for solar cells applications. *Phys. B* 566, 6 (2019).
32. S. Belfer, R. Fainchtain, Y. Purinson, and O. Kedem, Surface characterization by FTIR-ATR spectroscopy of polyethersulfone membranes-unmodified, modified and protein fouled. *J. Membr. Sci.* 172, 113 (2000).
33. A.F. Al-Hossainy, A. Ibrahim, and M.S. Zoromba, Synthesis and characterization of mixed metal oxide nanoparticles derived from Co–Cr layered double hydroxides and their thin films. *J. Mater. Sci. Mater. Electron.* 30, 11627–11642 (2019).
34. A. Givan, A. Loewenschuss, C.J. Nielsen, and M. Rozenberg, Formation of sulfuric acid and sulfur trioxide/water complex from photooxidation of hydrogen sulfide in solid oxygen at 15 K. *J. Mol. Struct.* 830, 21 (2007).
35. N. Almutlaq, A. Al-Hossainy, and M.S. Zoromba, Structural and energetics of weak non-covalent interactions in two chemically distinct classes of O/N-heterocycles: x-ray and theoretical exploration. *J. Mol. Struct.* 1227, 129712 (2021).
36. R. Morent, N. De Geyter, C. Leys, L. Gengembre, and E. Payen, Comparison between XPS- and FTIR-analysis of plasma-treated polypropylene film surfaces. *Surf. Interface Anal.* 40, 597 (2008).
37. A.F. Al-Hossainy, A. Ibrahim, and M.S. Zoromba, Development of the morphology and the band gap. *J. Mater. Sci. Mater. Electron.* 30, 11627 (2019).
38. P.K. Kuiri and J. Ghatak, Ion irradiation induced amorphization of SnO_2 nanoparticles embedded in SiO_2. *Vacuum* 85(2), 135–138 (2010).
39. S.K. Gautam and A. Chettah, *Nucl. Instrum. Methods Phys. Res. Sect. B Beam Interact. Mater. Atoms* 379, 224–229 (2016).
40. M.A. Arvizu, H.Y. Qu, U. Cindemir, and Z. Qiu, Electrochromic WO_3 thin films attain unprecedented durability by potentiostatic pretreatment. *J. Mater. Chem. A* 7(6), 2908–2918 (2019).
41. X. Zheng, F. Ren, S. Zhang, X. Zhang, H. Wu, X. Zhang, and C. Jiang, A general method for large-scale fabrication of semiconducting oxides with high SERS sensitivity. *ACS Appl. Mater. Interfaces* 9(16), 14534–14544 (2017).